Article

Evaluation of the Properties of an Electro-Sinter-Forged Bearing Steel

Róbert Bidulský[1,3], Federico Simone Gobber[1,*], Alessandro Fais[2], Jana Bidulská[4], and Marco Actis Grande[1]

[1] Politecnico di Torino; Department of applied science and technology (DISAT), Viale T. Michel 5, 15121 Alessandria, Italy; robert.bidulsky@polito.it (R.B.); federico.gobber@polito.it (F.S.G.); marco.actis@polito.it (M.A.G.)
[2] Epos s.r.l., Via Pavia 68/72 / 10098 — Rivoli (TO), Italy; af@eposintering.com (A.F.)
[3] Agency for the Support of Regional Development Kosice, Kosice Self-govering Region, Strojarenska 3, 040 01 Kosice, Slovakia; robert.bidulsky@vucke.sk
[4] Technical university of Kosice, Faculty of Materials, Metallurgy and Recycling, Institute of materials and quality engineering, Department of Plastic Deformation and Simulation Processes, Vysokoskolska 4, 04200, Kosice, Slovakia; jana.bidulska@tuke.sk (J.B.)
* Correspondence: Robert Bidulsky; robert.bidulsky@polito.it;

Abstract: In this study one of the most innovative sintering techniques up to date was evaluated: Electro-Sinter-Forging (ESF). Despite it has been proved to be effective in densifying several different metallic materials and composites, bearing steels such as 100Cr6 have never been processed so far. Pre-alloyed Astaloy CrM powders have been ad-mixed with either graphite or graphene and then processed by ESF to produce a 100Cr6 equivalent composition. Porosity has been evaluated by optical microscopy and compared to that one of 100Cr6 commercial samples. Mechanical properties such as hardness and transverse rupture strength were tested on samples produced by employing different process parameters and then submitted to different treatments (machining, heat treatment). The experimental characterization highlighted that porosity is the factor mostly affecting mechanical resistance of the samples, correlating linearly to the transverse rupture strength. Hardness on the other side does not correlate to the mechanical resistance because process related cracking has a higher effect on the final properties. Promising results were obtained that give room to the sinterability by ESF of materials difficult to sinter by conventional press and sinter techniques.

Keywords: electro sinter forging; powder metallurgy; capacitor discharge sintering; 100Cr6

1. Introduction

The sintering of metal powders is traditionally a purely thermal process where a previously pressed amount of powders called green, is densified in a furnace without applying further pressure. In sintering processes such as hot isostatic pressing (HIP), on the contrary, loose powders are densified by the concurrent effect of both high pressure and temperatures. Independently from the kind of thermal sintering technique employed, they are all suitable for obtaining both simple or complex shapes in a near final geometry, thus reducing mechanical work, material waste and costs [1-4]. All thermal sintering processes are characterized by long sintering cycles, performed in furnace, lasting several hours. Thermal sintering is commonly employed in the manufacture of gears and automotive components of small dimensions (almost 70% of the total powder metallurgy production [2-7]), electric contacts but also components for the aerospace sector such has turbine blades and rotors.

In order to reduce sintering time and to promote the processing of innovative metallic alloys and metal matrix composites (MMC), the so-called field assisted sintering techniques (FAST) have been developed in twentieth century [8,9]. Such technologies are characterized by a reduced processing time (from minutes down to milliseconds for FAST vs. hours for thermal sintering) that

 doi:10.20944/preprints202009.0364.v1

allows retaining a very fine microstructure even at the nanoscale. Among the materials commonly employed in the automotive sector and processed by powder metallurgy, there are no studies on the sinterability of 100Cr6 bearing steel. The characteristics of such grade of steel make it poorly sinterable, mainly due its very low compressibility: for this reason it would be very challenging to reach high density by conventional sintering techniques.

The 100Cr6 bearing steel (equivalent to the AISI 52100 grade) is characterized by high compression and wear resistance both adhesive and abrasive, with little mechanical deformations occurring even under high cyclic loading. From the heat treatment side, it is quenched in oil reaching hardness as high as 64 HRC. Such mechanical properties make the use of this material spread in the manufacture of wear resistant components such as eccentric gears, cylinders for small cold rolling mills; furthermore, over 90% of ball and cylinder bearings are made of 100Cr6.

Its chemical composition is characterized by the presence of high carbon (about 1%) and moderate chromium (1,5 %) that are responsible for the formation of chromium carbides. No rare or costly elements are present in this grade of steel, such characteristics make the 100Cr6 the most common grade employed in bearings production thanks also to a favorable balance between cost and mechanical properties.

1.1 Electro Sinter Forging (ESF)

The recent Electro-Sinter-Forging (ESF) or e-forging technique has demonstrated to be interesting and is gaining traction for precious alloys metals parts, cemented carbides tools, memory shape alloys and steels [10-14]. The intrinsic advantages of ESF led to the emergence of novel applications and uses: one machine is used for forming and sintering to near net shape in a very rapid productive process employing less than 10 seconds per each part produced. The amount of energy required is limited and this helps in reducing costs and pollutants, finally if compared to conventional casting [15] or cutting techniques [16], ESF has low wear of tooling and a generally higher precision of parts produced. The technical and manufacturing advantages of these techniques combine with the possibility of creating innovative materials such as metal composites and diamond composites with novel, high performance, properties and extremely high densities. Electro-Sinter-Forging (ESF) is simple: a mechanical pulse is superimposed to an electrical one in a die that is previously loaded with the powders.

A capacitor bank originates the electrical pulse at high voltage than a transformer raises the current and lowers the voltage. The electro-magnetic discharge is synchronized to the mechanical impulse so that energy is transferred just after reaching a set level of pressure, this guarantees an homogeneous flow of current through the powders. The second role of the mechanical pressure is compensating the powder shrinkage during sintering, for this reason mechanical pressure is raised when the electro-magnetic energy is transferred through the powders. After holding in pressure from a few milliseconds to, usually 1-3 s the powders while consolidating, the upper plunger is automatically drawn out of the die and the lower plunger is moved to the upper part of the die in order to extract the sintered piece from the die assembly.

Preprints (www.preprints.org) | NOT PEER-REVIEWED | Posted: 16 September 2020 doi:10.20944/preprints202009.0364.v1

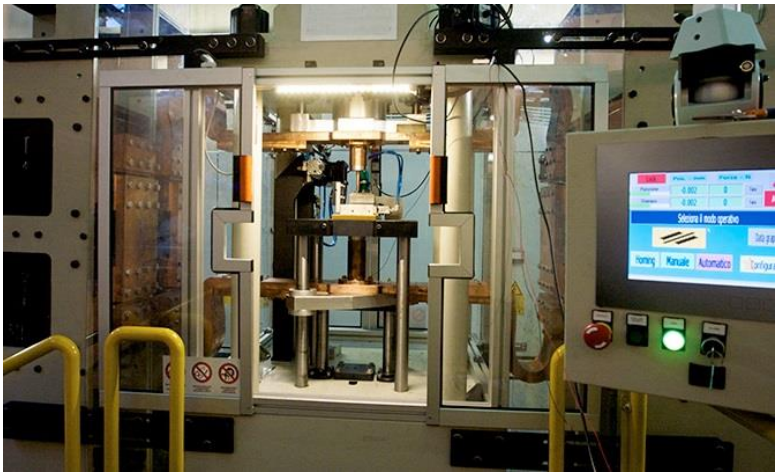

Figure 1. Photo of an Electro-sinter-forging system.

In this study a steel with a 100Cr6 equivalent composition has been sintered by ESF in order to prove the efficacy of this peculiar capacitive discharge sintering (CDS) technology in processing a bearing steel grade that normally is not processed via conventional thermal sintering techniques.

2. Materials and Methods

Prealloyed Astaloy CrM water atomized powders by Hoganas have been used as raw material for the study [17]. The chemical composition of the starting powders is given in Table 1.

Table 1. Chemical composition of the Astaloy CrM powders.

C	Cr	Mo	Fe
< 0,01	3,00	0,50	Bal.

The total Oxygen content reported by the powder supplier is 0,2%, such indication is important for powders made by water atomization because it can give a fruitful insight on sinterability. ESF is a sintering process activated by electric energy the higher the oxidation levels of the powders the higher the risk that the current flow is hindered. The Cr content in the powders is higher with respect to conventional casting/forged 100Cr6, this can contribute to the formation of a higher content of Cr based carbides that can confer higher wear resistance (especially abrasive wear resistance) to the sintered material.

For the analysis carried out in this study, rectangular shaped samples were produced by ESF (20 X 10 X 4 mm) employing the process parameters and the post processing reported in Table 2. These samples have than been compared to cylindrical shaped commercial samples (10 mm diameter and 4 mm thick) in terms of porosity, microstructure and mechanical properties. Due to the low carbon content of the Astaloy CrM powders, carbon was added either as graphite or graphene to the powders in order to reach a fraction between 0,95 and 1% wt. comparable to 100Cr6. A turbula mixer, with small amounts of hepthane was used to incorporate graphene with the Astaloy CrM powders while the graphite-containing samples were supplied as a pre-mix by the supplier.

Table 2. Process parameters and post – sintering treatments employed in this study.

Preprints (www.preprints.org) | NOT PEER-REVIEWED | Posted: 16 September 2020 doi:10.20944/preprints202009.0364.v1

Sample	Powder	SEI [kJ/g]	P_{start} [MPa]	P_{max} [MPa]	Finishing operations	Heat treatment
Y	100Cr6 commercial	-	-	-	Face milled	Yes
Z	100Cr6 commercial	-	-	-	Face milled	No
B	Astaloy CrM + graphite (0,97% C)	2,1	20	220	-	No
C	Astaloy CrM + graphite (0,97% C)	2,1	20	220	Grinded (0,05 mm)	No
D	Astaloy CrM + graphite (0,97% C)	2,1	20	220	Grinded (0,05 mm)	Yes, after grinding
E	Astaloy CrM + graphene (0,97% C)	1,9	20	235	-	Yes
F	Astaloy CrM + graphene (0,97% C)	2,2	20	281	-	Yes
G	Astaloy CrM + graphene (0,97% C)	2,2	20	279	-	No

After sintering, metallographic preparation was done by grinding with SiC based abrasive papers (from 200 to 2400 grit) and then polishing with cloths soaked with diamond based suspensions (from 3 down to 1 μm). Both directions, parallel and perpendicular to the loading axis of the ESF machine were analyzed. Light optical micrograph have been obtained through a Leica MEF4M and porosity was analysed by image analysis through the software Qwin. Both micro and macro hardness were performed to evaluate the influence of porosity on the microstructure. Vickers micro hardenss was tested through a Leica VMHT with 200 and 500 gf load while macro hardness was tested on an EMCOtest M4U 025 adopting the HRN test method. Measured values were then converted by the machine itself to the HRC scale. Macro hardness was measured on unmounted samples in order to prevent the risk of the mounting resin to affect the measurement. By adopting this micro/macro hardness testing approach, the effect of porosity on microstructure could be separated. Mechanical properties were tested with three point bending test, as commonly done for PM materials. Transverse rupture strengths were measured on samples 20 X 10 X 4 mm with 15 mm distance between the constraints, a 20 N pre-load and a 0,08 mm/min elongation rate.

3. Results and discussion

3.1 Microhardness and Macrohardess

Microhardness testing was performed at ambient temperature and the results for the tested samples are reported in Figure 2. The distinction between Z and XY directions is made referring to the pressing direction in the ESF machine, being Z the pressing direction and XY the plane perpendicular to it.

Preprints (www.preprints.org) | NOT PEER-REVIEWED | Posted: 16 September 2020 doi:10.20944/preprints202009.0364.v1

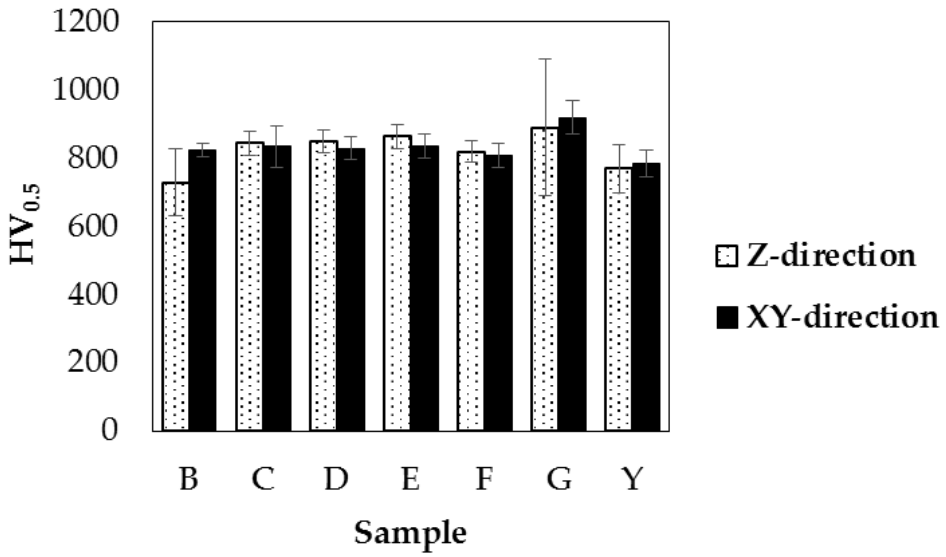

Figure 2. Bar chart reporting the microhardness values of the different samples measured perpendicularly and parallel to the pressing direction.

The measured microhardness values of the ESFed samples are higher on an average value with respect to the commercial ones (Y sample in Figure 2) except for sample B. The difference among the samples is confirmed by the ANOVA general linear model (P = 0,000; F = 6,65) for α = 95% confidence level. Furthermore, by comparing samples B, C and D having the same sintering parameters it is possible to conclude that the heat treatment after ESF does not influence the values of hardness while grinding increases the average microhardness probably due to the removal of the outermost layer, where residual pores concentrate more [18].

By comparing samples B and C, that differ only for the grinding, applied on sample C, a significant increase in the microhardness measured along the pressing direction on the grinded sample can be noticed. Samples G and F, with addition of graphene show lower microhardness only for the heat treated sample despite sintering conditions were comparable to those applied on samples B to D and higher values for the as-sintered sample. Despite the values of microhardness slightly differ for all samples depending on the direction analyzed, it is just for sample B that this difference is significant from a statistical point of view. From this analysis a first assessment can be drawn: the use of graphene does not seem to carry important benefits, especially in a cost/benefit prospective. Its cost is 30 times higher than graphite but the mechanical properties delivered are only blandly superior.

Macroscopic properties are shown by the HRC measurements reported in **Figure 3**. Due to pores at the surface, samples E and G are significantly different. Such porosities cause a drop in the measured hardness while they are not affecting Vickers microhardness. Sample F containing graphene and heat treated reaches the maximum average macro hardness, whereas sample E which also contains graphene and was heat treated (but not optimized in the ESF process parameters) contains a higher porosity which is responsible for a lower macro hardness.

Preprints (www.preprints.org) | NOT PEER-REVIEWED | Posted: 16 September 2020 doi:10.20944/preprints202009.0364.v1

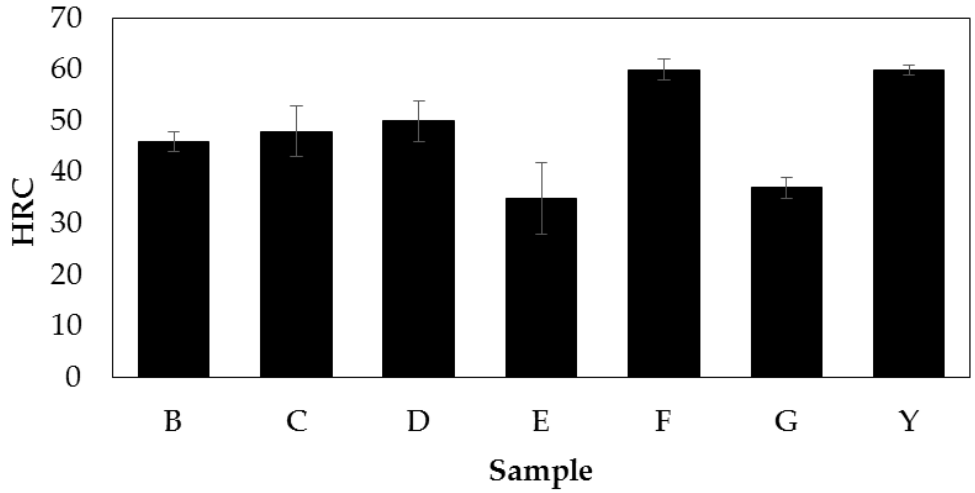

Figure 3. Bar chart representing the macroscopic hardness of the samples analysed.

Porosity was measured from image analysis and the results for the different direction analysed are reported in **Figure 4**. Commercial samples of 100Cr6 from casting/forging were not included in the results because their porosity was null. Porosity measured in the pressing direction (z direction) is higher than porosity in the XY, this behavior can be attributed to the deformation direction during pressing.

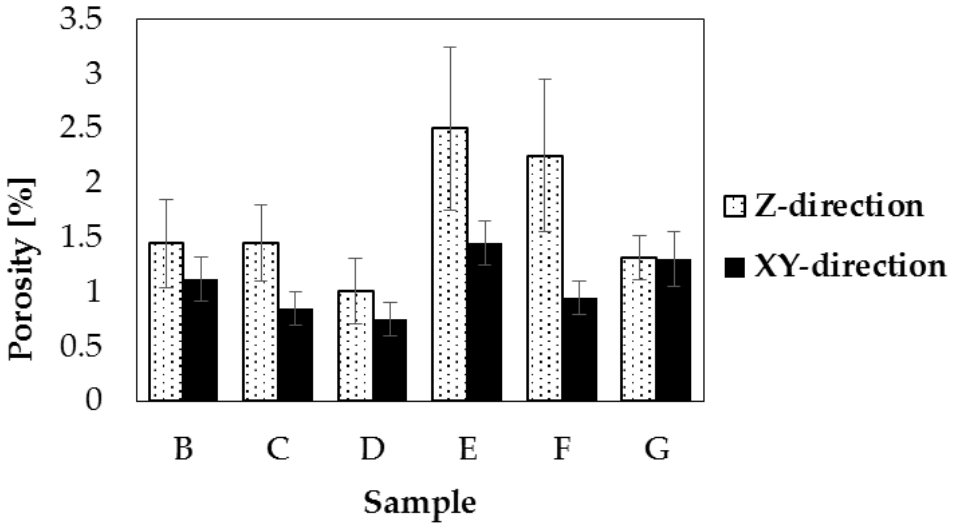

Figure 4. Bar chart representing the results of porosity measured on ESF samples.

The evaluation of porosity was done after polishing the samples progressively and analyzing porosity over different layers of the sample to measure a volumic average. Porosity roughly represents the fraction of void volume over total volume. Pore structures like pore size, morphology and distribution of porosity within the pressed part present critical items in the load bearing sections, which mean the main controlling mechanism of the mechanical properties result [20-23]

A significant aspect to point out is that graphene containing samples have a higher porosity, this evidence is another clue to consider if a choice between graphite and graphene as carbonaceous element has to be made. The micrographs of **Figure 5a** reveals that towards the edge of the sample, along the Z direction, a relevant degree of porosity of approximately 50 – 100 µm is detectable in sample E.

 doi:10.20944/preprints202009.0364.v1

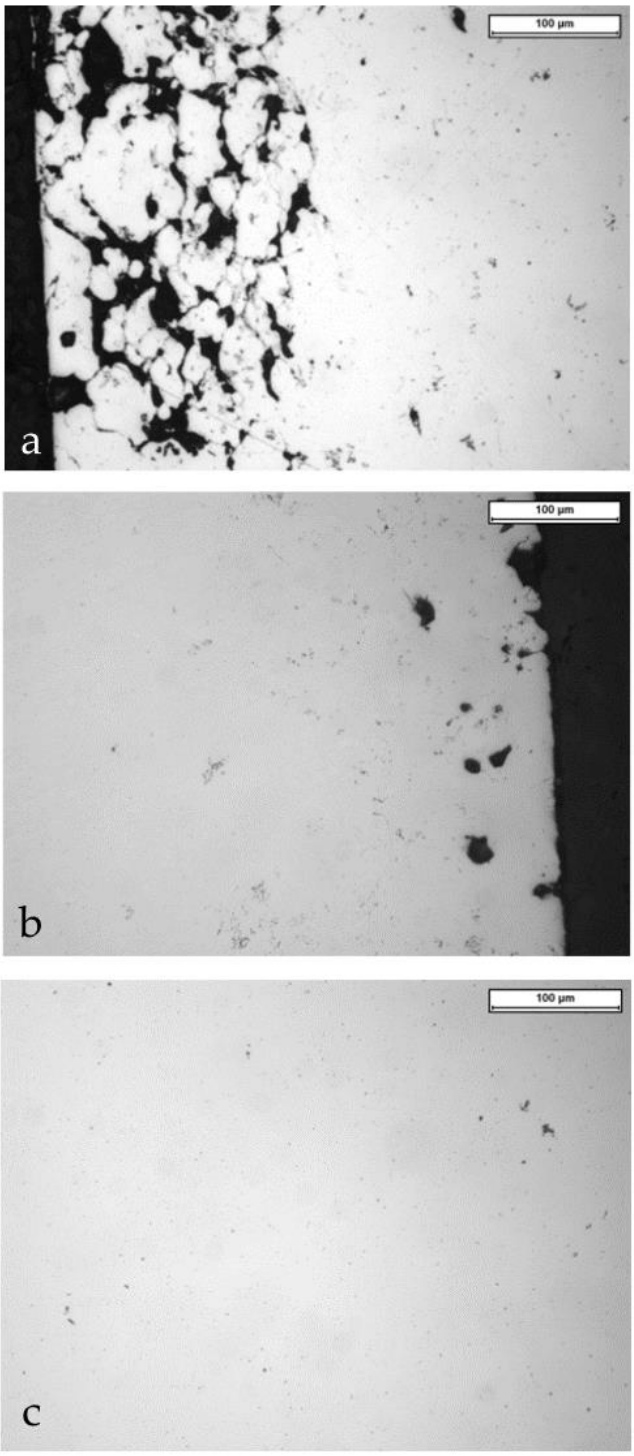

Figure 5. Optical micrograph of samples obtained through ESF. a) edge of sample E along direction Z, b) edge of sample B along direction Z, c) core of sample F.

Figure 5a explains the high level of porosity measured. Similar considerations can be made for sample F, whose edge is similar to that of E. The core of sample F, on the other hand is fully dense (Figure 5c), confirming that materials sintered via ESF can suffer from porosity in the edge but not at the core.

Currently, process parameters need to be further fine tuned because excessive porosity could lead to early failure of the sintered component although a grinding of 100 µm is be enough to remove the porous layer.

A correlation was verified between TRS and porosity (**Figure 6**), it seems that the porosity in the direction perpendicular to the plungers (XZ-plane) has a relevant effect on TRS. Porosity measured

Preprints (www.preprints.org) | NOT PEER-REVIEWED | Posted: 16 September 2020 doi:10.20944/preprints202009.0364.v1

along the XZ – plane is much more significant than porosity measured along the XY plane as justified by the R-squared value of 0,7455. From this observation it can be said that an increasing level of porosity negatively affects mechanical properties and from a provisional point of view it is possible to predetermine with a certain accuracy the TRS of an ESFed Astaloy CrM sample, based on a linear relation.

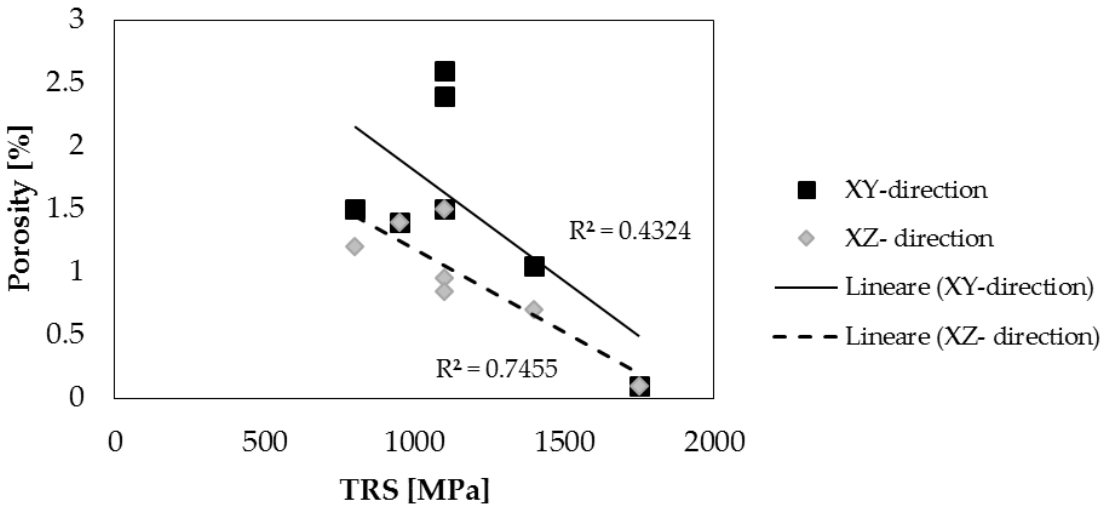

Figure 6. Optical micrograph of samples obtained through ESF. a) edge of sample E along direction Z, b) edge of sample B along direction Z, c) core of sample F.

Chemical etching with Nital 2 evidenced the microstructure of the samples, such microstructures represent the traces of the thermal history that the loose compact of powders have undergone during electro sinter forging. Samples B and G, whose microstructure are reported in **Figure 7**, were molten in the core but not at the surface. If the whole compact of powders had molten during ESF, the high impulsive forces applied by the plungers would have squeezed the liquid out of the die thus damaging the tooling. The choice of the process parameters (Pmax, Pstart and SEI) is a crucial part of ESF to prevent undesired failures and compromission of the dies. On one side, too low values of the process parameters are not effective in densifying the compact of powders while too high parameters (especially SEI) can melt the whole compact of powders with the risk of welding the material under process and the die.

The surface layer (approx. 150 μm) is mainly ferritic (light coloured) having a certain degree of retained pores (**Figure 7a**). Such observation is not intuitive if we consider the composition of the Astaloy CrM + graphite. The microstructure of a steel with 1% carbon would mainly be made of martensite or pearlite and no isolate ferrite should be present, but in this case the temperature at the edge of the ESFed sample does not reach the limit for diffusion and alloying to occur. The temperature reached at the interface between plungers and powders is lower with respect to that reached at the core of the sample thus the mix of Astaloy CrM and graphite does not alloy completely, with graphite and powders that stay separate leading to a higher degree of surface porosity.

Moving towards the core of the sample it is possible to observe a dendritic like microstructure, with dendrites developing towards the direction where heat is dissipated. Such microstructure is caused by the high amount of heat that locally melts the internal part of the loose powders contained in the die and then is dissipated towards the plungers and the die itself. The core is melted instantaneously and rapidly solidified again.

Preprints (www.preprints.org) | NOT PEER-REVIEWED | Posted: 16 September 2020 doi:10.20944/preprints202009.0364.v1

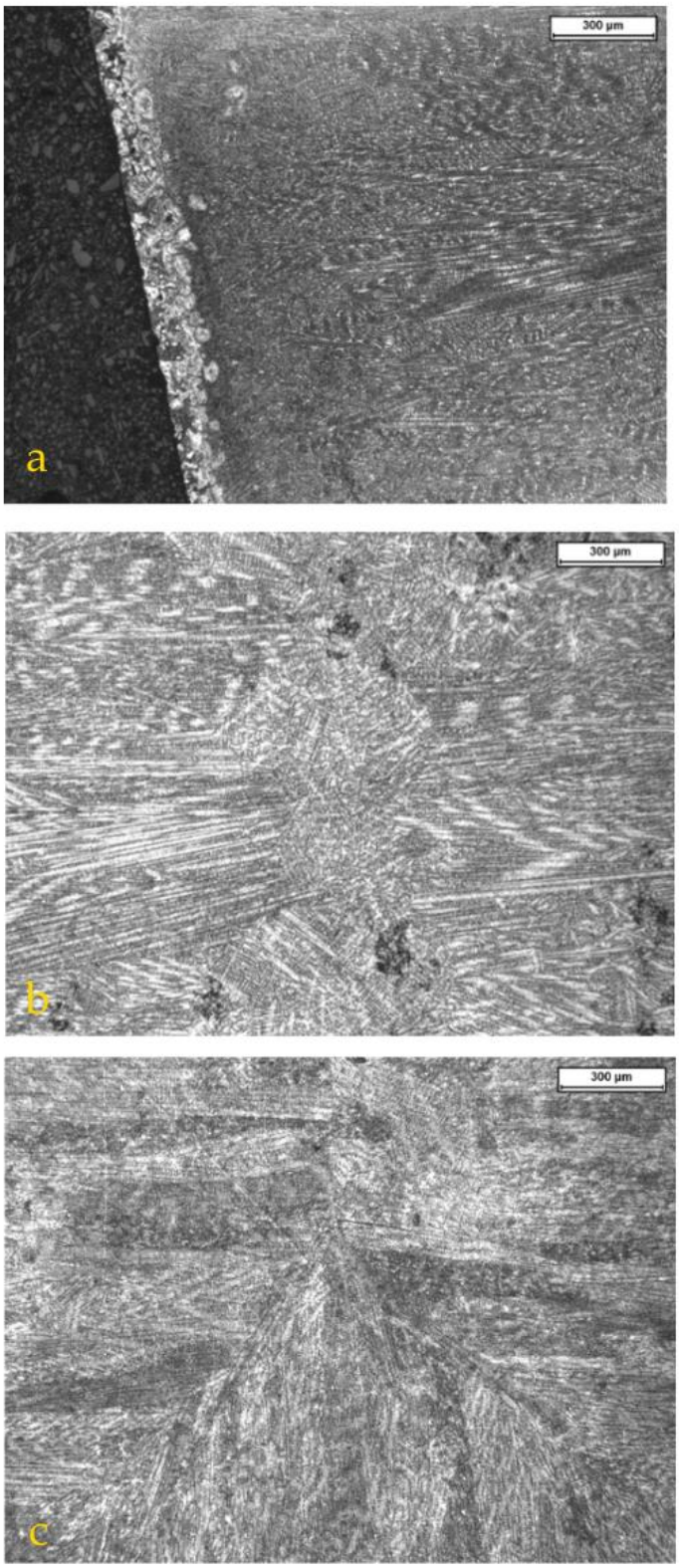

Figure 7. Optical micrograph of the microstructure of samples obtained through ESF on the XZ plane. a) edge of sample B, b) core of sample B, c) core of sample G.

5. Conclusions

In this experimental work an innovative electrically assisted fast sintering technique named ESF was used to densify a steel grade with a composition close to that of AISI 51200, commonly known as 100Cr6. For the first time it was possible to sinter this material that conventionally is obtained by

casting/forging only. Such result can be disruptive considering the very fast production rate of ESF, With this technique small components can be successfully produced with near net shape.
With particular reference to the experimental data presented, the following points represent the main achievement reported towards this work:

- Astaloy CrM powders were successfully mixed and then alloyed with graphite or graphene to obtain samples with the same carbon content of 100Cr6 bearing steel. Both graphite and graphene are effective in raising the carbon content in the starting powders but based on the compromise between cost and performance of the materials, it is reasonable to suppose that graphite can be a much better and affordable solution.

- Typical microstructures obtained by ESF were observed in the sintered samples, presenting a core – rim microstructure distinctive of ESFed materials. By properly tuning the process parameters a fully dense material is obtainable but a cautious evaluation has to be done in order to densify the material without damaging the machine. Surface finishing the sintered samples by grinding has to be taken into account in order to remove the porosity that concentrates in the outermost layers of material.

- High values of hardness, compatible with a quenched material were observed after ESF. Heat treating the material was not effective to further increase its hardness.

- A linear correlation between porosity on the XZ plane and TRS was found for the tested samples. With porosity negatively affecting the mechanical properties.

Author Contributions: "writing—original draft preparation, F.S.G.; A.F. ; writing—review and editing, M.A.G and J.B.; investigation, F.S.G.; R.B. and J.B.; supervision, A.F. and M.A.G.; methodology, M.A.G. and A.F.; validation, J.B., M.A.G.; formal analysis, F.S.G.; resources, A.F. and M.A.G; funding acquisition, J.B.".

Funding: "This research was partially co-funded by VEGA, grant number 1/0599/18".

Acknowledgments: The authors would like to thank Mr. Luca Capurso for his precious work in the execution of the analysis.

Conflicts of Interest: "The authors declare no conflict of interest."

References

1. German, R.M. *Powder Metallurgy Science*. Metal Powder Industries Federation: Princeton, USA, 1994; ISBN: 0918404606.
2. Salak, A. *Ferrous Powder Metallurgy*. Cambridge International Science Publishing: Cambridge, England, 1997; ISBN: 1898326037.
3. Phuong, D.D., Trung, T.B., Chung, L.D., Hung, T.B. Effect of binder composition and sintering temperature on the microstructure and mechanical properties of WC-7(Ni,Fe) hard alloys prepared by free capsule hip technique. *Acta Metall. Slovaca* **2019**, *25*, 123-129, doi: 10.12776/ams.v25i2.1270.
4. German, R.M. *Sintering: From Empirical Observations to Scientific Principles*. Butterworth-Heinemann: Oxford, England, 2014; doi:10.1016/C2012-0-00717-X.
5. Dang, K.Q., Nguyen, Y.N., Hoang, Q.A., Van Tran, H., Nguyen, M.C., Van Pham, H., Le, H.M. Densification and mechanical properties of FeMn13-TiC composites fabricated by pulsed electric current sintering process. *Acta Metall. Slovaca* **2018,** *24*, 273-279, doi: 10.12776/ams.v24i4.1195.
6. Gloria, A., Montanari, R., Richetta, M., Varone, A. Alloys for aeronautic applications: State of the art and perspectives. *Metals* **2019**, *9*, 662, doi: 10.3390/met9060662.
7. Jones, P., Buckley-Golder, K., Lawcock, R., Shivanath, R. Densification strategies for high endurance P/M components. *International Journal of Powder Metallurgy* **1997**, *33*, 37-44.

8. Kruszewski, M.J., Zybała, R., Ciupiński, Ł., Chmielewski, M., Adamczyk-Cieślak, B., Michalski, A., Rajska, M., Kurzydłowski, K.J. Microstructure and Thermoelectric Properties of Bulk Cobalt Antimonide (CoSb3) Skutterudites Obtained by Pulse Plasma Sintering. *J. Electron. Mater.* **2016**, *45*, 1369–1376, doi: 10.1007/s11664-015-4037-5.
9. Shen, B., Inoue, A. Fabrication of large-size Fe-based glassy cores with good soft magnetic properties by spark plasma sintering. *J. Mater. Res.* **2003**, *18*, 2115–2121. DOI:10.1557/JMR.2003.0297.
10. Yurlova, M.S., Demenyuk, V.D., Lebedeva, L.Yu., Dudina, D.V., Grigoryev, E.G. Olevsky, E.A. Electric pulse consolidation: An alternative to spark plasma sintering. *Journal of Materials Science* **2014**, *49*, 952-985, doi:10.1007/s10853-013-7805-8.
11. Fais, A. A faster FAST: Electro-Sinter-Forging. *Met. Powder Rep.* **2018**, *73*, 80–86, 2018, doi: 10.1016/j.mprp.2017.06.001.
12. Forno, I., Actis Grande, M., Fais, A. On the application of Electro-sinter-forging to the sintering of high-karatage gold powders. *Gold Bull.* **2015**, *48*, 127–133, doi: 10.1007/s13404-015-0169-x.
13. Balagna, C., Fais, A., Brunelli, K., Peruzzo, L., Spriano, S. Effect of heat treatments on a Ni-Ti alloy sintered by Electro-Sinter-Forging. *J. Alloys Compd.* **2017**, *726*, 338–347, doi: 10.1016/j.jallcom.2017.07.311.
14. Fais, A., Actis Grande, M., Forno, I. Influence of processing parameters on the mechanical properties of Electro-Sinter-Forged iron based powders. *Mater. Des.* **2016**, *93*, 458-466, doi: 10.1016/j.matdes.2015.12.142.
15. Fais, A. Advancements in single pulse high speed sintering technologies: Electro-sinter-forging. Int. Powder Metall. Congr. Exhib. Euro PM **2013**, 1-6.
16. Gobber, F.S., Pisa, A.G., Ugues, D., Rosso, M. Design of a Test Rig for the Characterization of Thermal Fatigue and Soldering Resistance of the Surfaces of Tool Steels for High-Pressure Die-Casting Dies. *Steel Res. Int.* **2020**, *91*, 1900480, doi: 10.1002/srin.201900480
17. Rosso, M., Gobber. F.S., Fracchia, E. Focus on Carbide-Tipped Circular Saws when Cutting Stainless Steel and Special Alloys," *Adv. Mater. Res.* **2015**, *1114*, 13–21.
18. Lindberg, C., Johansson, B., Maroli, B. Mechanical properties of warm compacted Astaloy CrM. *Adv. Powder Metall. Part. Mater.* **2000**, *3*, 76–81, 2000.
19. Balagna, C., Fais, A., Brunelli, K., Peruzzo, L., Horynová, M., Čelko, L., Spriano, S. Electro-sinter-forged Ni-Ti alloy. *Intermetallics* 2016, *68*, 31-41, doi: 10.1016/j.intermet.2015.08.016.
20. Bidulská, J., Bidulský, R., Grande, M.A., Kvačkaj, T. Different formation routes of pore structure in aluminum powder metallurgy alloy. *Materials*, **2019**, *12*, 3724, doi: 10.3390/ma12223724.
21. Petrousek, P., Kvackaj, T., Kocisko, R., Bidulska, J., Luptak, M., Manfredi, D., Grande, M.A., Bidulsky, R. Influence of cryorolling on properties of L-PBF 316l stainless steel tested at 298K and 77K. *Acta Metall. Slovaca*, **2019**, *25*, 283-290, doi: 10.12776/ams.v25i4.1366.
22. Bidulská, J., Kvackaj, T., Pokorný, I., Bidulský, R., Actis Grande, M. Identification of the critical pore sizes in sintered and ECAPed aluminium 6XXX alloy. *Arch. Metall. Mater.* **2013**, *58*, 371-375, doi: 10.2478/amm-2013-0002.
23. Bidulská, J., Kvačkaj, T., Bidulský, R., Grande, M.A., Lityńska-Dobrzyńska, L., Dutkiewicz, J. The densification phenomena in powder metallurgy aluminium alloy Al-Zn-Mg-Cu. *Chem. Listy* **2011**, *105*, s471-s473, doi: 10.2478/amm-2013-0002.